Phenomenological model of thermal transport in films of carbon nanotubes and hetero-nanotubes

Pengyingkai Wang[1], Ya Feng[1], Rong Xiang[1], Taiki Inoue[1] Anton Anisimov[2], Esko I. Kauppinen[3], Shohei Chiashi[1], Shigeo Maruyama[1*]

[1] Department of Mechanical Engineering, The University of Tokyo, 7-3-1 Hongo, Bunkyo-ku, Tokyo 113-8656, Japan
[2] Canatu, Ltd., Konalankuja 5, FI-00390 Helsinki, Finland
[3] Department of Applied Physics, Aalto University School of Science, 15100, FI-00076 Aalto, Finland

Email address: maruyama@photon.t.u-tokyo.ac.jp

ABSTRACT

Thermal properties of individual single-walled carbon nanotubes (SWCNTs) have been well documented in the literature after decades' intensive studies. However, when SWCNTs form a macroscale assembly, the thermal transport in these complex structures usually not only depends on the property of individual tube, but also affected and sometime dominated by inner structural details, e.g. bundles and junctions. In this work, we first performed an experimental measurement on thermal conductivities of individual SWCNT bundles with different sizes using a suspended micro thermometer. The results, together with the data we obtained in a previous work, give a complete experimental understanding on the effect of bundling on the thermal conductivity of SWCNTs. With these quantitative understandings, we propose a phenomenological model to describe the thermal transport in two-dimensional (2D) SWCNT films. A term called line density is defined to describe the effective thermal transport channels in this complex 2D network. Along with geometry statistics and film transparency obtained by experiments, thermal conductance of SWCNTs are estimated, and the effects of bundle length, diameter and contact conductance are systematically discussed. Finally, we extend this model to explain the thermal transport in 2D networks of one-dimensional van der Waals heterostructures, which are coaxial hetero-nanotubes we recently synthesized using SWCNTs as the template. This extended model suggests that the contribution of BNNTs to the overall performance of a SWCNT-BNNT heterostructure film depends on the transparency of the original SWCNT film. The increase of the thermal conductance for a highly transparent film is estimated to be larger than that in a less transparent film, which shows a good agreement with our experimental observations and proves the validity of the proposed phenomenological model.

Keywords: network film model, single-walled carbon nanotube film, boron nitride nanotube, van der Waals heterostructure, thermal conductance

1. Introduction

Low-dimensional nanomaterials have been extensively studied in the past decades because of their unique geometric arrangement and thereby distinctive properties [1-4]. Carbon nanotube (CNT), as one classic one-dimensional (1D) material, was proven to have excellent electrical, optical, mechanical and thermal properties. In addition to the form of individual tubes, CNTs can be readily integrated into two-dimensional (2D) or three-dimensional (3D) macro-assemblies by *in situ* growth or post-growth fabrication processes [5-8]. A film of randomly networked CNTs, which is a representative form for 2D assemblies, can now be produced in large area and widely utilized for applications such as transparent conductive film, solar cells, sensors and thermal managements [9-11]. Although the property of an individual CNT has been well documented after 30 years' intensive studies, the properties of macro-assemblies are usually more complex. Their performances in applications are affected by not only individual tubes but also inner structures, such as defects, junctions, contacts and bundles. Elucidating these effects by experiments usually faces many technical challenges, so modelling by a numerical or theoretical approach is important to understand the complex behavior inside of a macro-assembly. For example, investigation of the thermal transport in a network structure needs a proper model of CNT bundles, a common building block for two- and three-dimensional CNT assemblies [12].

In previous studies, various models have been developed to describe the thermal transport mechanism in complex structures of CNT assemblies [2]. Kumar et al. [13] used a diffusive transport model to explore the thermal conductivity of 2D nanotube composite. Their work showed the limitation of effective medium approximation method [14] and emphasized the importance of inter-tube interactions at high volume fractions. Zhigilei et al. [15] developed both analytical expressions and numerical models of randomly distributed CNT networks. Using soft-core approach and based on geometry of the film, thermal conductivity could be determined by the intrinsic thermal conductance of CNT and interfacial thermal conductance between CNTs. Behnam et al. [16] generated a random stick network with Monte Carlo process and estimated the electrical conductivity of CNT film with Kirchoff's current law accurately. Except for the detailed models, some researchers have treated CNT assemblies as a whole entity [17-20]. In the aforementioned models, inter-tube junctions are the core factor for modelling CNT films. However, due to the difficulty in accurate modeling and the difference in simulation conditions, the reported inter-tube junction conductance has very large deviations. Moreover, CNT bundles, rather than individual CNTs, are the basic component in such networks but bundle effects were vaguely discussed previously. Besides, CNT networks have been recently used as the template to synthesize a 1D van der Waals heterostructure, which is a coaxial multi-walled nanotube consisting of different materials. [1, 3, 21, 22] Although we have confirmed an improved thermal conductance after the CNTs are coated by boron nitride nanotubes (BNNTs), the mechanism is not fully understood and the existing models can hardly describe the transport in such complex structures.

Therefore, the focus of this study is to find out a simple but effective model to evaluate the thermal transport of a 2D film, which is composed of purely CNTs or CNT based van der Waals heterostructures. The basis of this research is the dependence of thermal conductivity of single-walled CNT (SWCNT) bundles on bundle size. Firstly, the quantitative dependence was derived, as an extension of our previous research [12], by additional measurements of individual SWCNT bundles using a suspended micro thermometer. In the second part, a practical model is proposed for SWCNT films. This model is based on results of bundle effect obtained in the first part, together with our additional experimental investigations on the structure of our 2D SWCNT films. Different from previous studies, only the two junctions near the ends of CNT are considered. Besides, instead of a complete calculation of every thermal transport path, only the ones consisting of long CNTs are considered as dominant in this model. Thermal conductance could be roughly evaluated with geometry statistics of the SWCNT film. With the experimental corroboration, this model is further developed to van der Waals heterostructure films to verify its effectiveness. The structure-sensitive thermal conductance revealed in the model points out the feasibility of controlling and directing heat flow in nano- and macroscale SWCNT assemblies pertinently.

2. Thermal transport model of SWCNT film

CNT film is a 2D structure where CNT or CNT bundles are randomly distributed into a network. Models have been developed on such random networks in order to reveal the electrical transport mechanism while tuning conditions like alignment and area density.[23, 24]

In this study, the curvature of CNT or CNT bundle in the tube axis direction is ignored, as shown in Fig1 (a). The square film with size of $L \times L$ is placed between heat source T_H and heat sink T_C. The SWCNTs and SWCNT bundles are randomly distributed and form paths that can conduct heat from one side to the other. Among these paths, the ones consisting of long SWCNTs with less junctions contribute more to the overall thermal transport because junctions greatly impede phonon transport greatly. In Fig1 (a), the red path will possess higher thermal conductance than the green one.

Besides, the junctions at intermediate positions of a bundle have little influence on thermal transport, so they are ignored [25]. Therefore, the important thermal transport channels are those with least number of junctions. Fig.1 (b) is one example of the path where SWCNT and SWCNT bundles are connecting end to end from left to right. "B" and "J" denote bundle and junction in the figure and l, d are the length and diameter of the bundle. The equivalent thermal circuit is illustrated below. In this way, the thermal conductance G of the film can be treated as the production of path thermal conductance G_P and the number of paths N_P, shown as Eq. (1). The thermal circuit suggests that bundle thermal conductance and contact thermal conductance are the two main parts in the model.

$$G = G_P \times N_P \qquad \text{Eq. (1)}$$

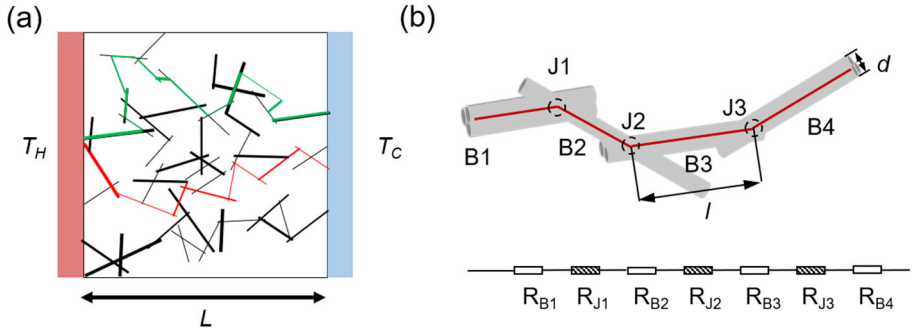

Figure 1. (a) A schematic illustration of the SWCNT film. The red and green paths are two examples through which heat transfers from hot side to cold side. (b) Schematic illustration of a conducting path. Length of the distance between two contacts is l and diameter of bundle is d. The lower part is the equivalent thermal resistance model of the path, where footprint "B" denotes bundle and "J" denotes contact.

2.1. Thermal transport in SWCNT bundle.

In this section, the basic component in thermal transport path, SWCNT bundle will be discussed based on a previous experiment study [12],. Bundle size is defined as the number of SWCNTs in a bundle and the thermal conductivity has been measured in a wide temperature range. Based on our previous study, several more samples have been tested and the SWCNT bundle thermal transport model has been updated. Characterization of the new samples is presented in Supporting Information S1. The experiment results are shown in Fig. 2 (a) by colored dots. The thermal conductivity of a bundle is only slightly lower than individual tube if the bundle size is two, but the value quickly decreases when the number of CNT in the bundle increases. When the bundle size reaches above ten, thermal conductivity tends to saturate to a value, which is comparable to that of aligned CNT films[4] .

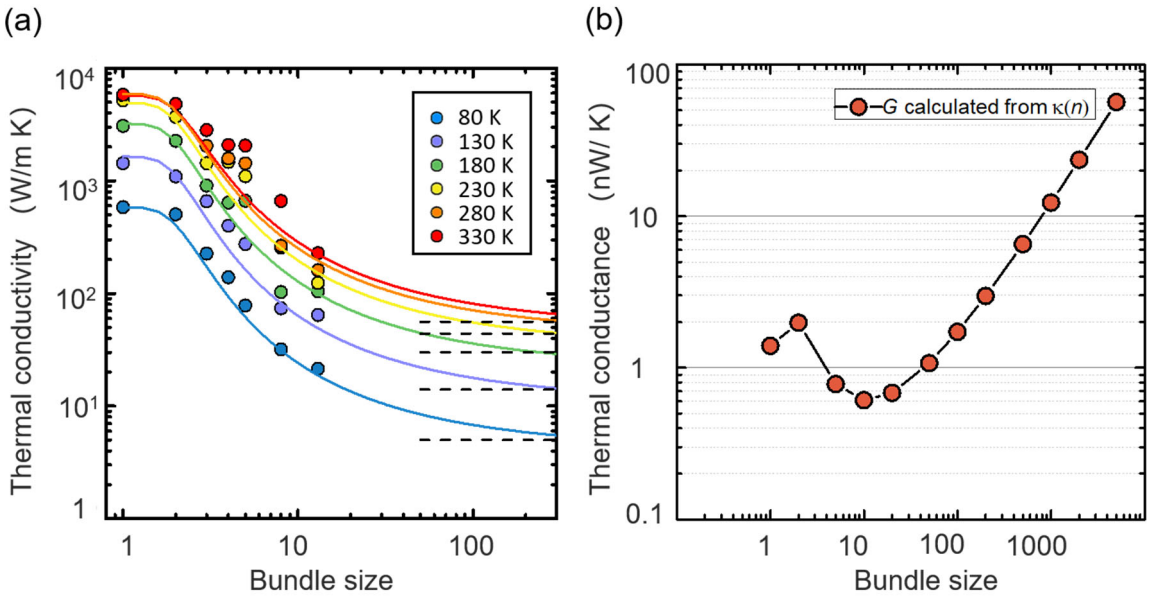

Figure 2. (a) Colored dots in the figure are thermal conductivity plotted against bundle size at different temperatures. The experiment data are fitted with Eq. 2 with same color. The dashed black lines are the bulk thermal conductivities when bundle size reaches infinite. (b) Dependence of thermal conductance on the bundle size. With increase in the bundle size, thermal conducting channels as well as phonon scattering increase synchronously and reach balance at bundle size about 15.

In our previous model, simple kinetic theory is employed to describe the transport mechanism with different sized bundle, but the bundle size has not been discussed sufficiently. [12] In addition to the previous model, bundle size is taken as a parameter to show the intensity of phonon scattering. Bundle thermal conductivity κ_{bu} is decided by bundle size n_b, length l and temperature t and is expressed by Eq. (2).

$$\kappa_{bu}(n_b, l, t) = \frac{\kappa_{is}(l,t)}{1+A(t)*\varphi(n_b)^4} \quad \text{Eq. (2)}$$

In this equation, $\kappa_{is}$is the thermal conductivity of individual SWCNT, fitted by the model from E. Pop's previous work [26] based on the experimental result in this study. More details are in Supporting information S2. $A(t)$ is a temperature dependent parameter and $\varphi(n_b)$ reflects the non-linear relationship between SWCNT bundle and SWCNT. This equation could be expanded by adjusting the temperature, diameter or length of the bundle. Fig. 2(b) shows the thermal conductance varies with bundle size, indicating that the relationship is not linear. The competition between more SWCNT and intense phonon scattering leads to a minimum thermal conductance at bundle size about 15.

Considering that the bundle size in the film is random and difficult to determine by current techniques, diameter is used to give a rough estimation of the bundle size, assuming that each bundle is closely packed, resulting in the hexagonal cross-section. In this way, the $\kappa_{bu}(n_b, l, t)$ becoms $\kappa_{bu}(d_b, l, t)$ SWCNT film with transparency of 87% is examined by transmission electron microscopy (TEM) and diameters of 100 bundles are measured. It should be noted here that the SWCNT films are exactly the same ones reported in Ref. 3 for a fair comparison. Frequency histogram is presented in Supporting information S3, and the diameter distribution of the bundles in this film is denoted as " d_b " and it obeys lognormal, $d_b \sim Lognormal(2.29, 0.29^2)$. Length distribution of the SWCNT bundles is adopted from Ref 5 and 6.

2.2. Mean model

Contact conductance per area $G_C$has been discussed a lot in previous researches [4, 18, 19, 27-33], but the reported values scatter from 5 to over 100 MW/m^{2}K. Despite the aforementioned reasons, contact area between SWCNT is also difficult to define. (Supporting information 4). In this work, a moderate value of 40 MW/m^{2}K is chosen as contact conductance per area, denoted as G_C. The contact area S is roughly calculated given each bundle is in touch with another two bundles and is contact angle dependent. Therefore, junction conductance G_j of two bundles with contacting angle of θ is expressed as $G_j = G_C \cdot S/\sin\theta$. Length of the SWCNTs also follows lognormal distribution, and the average length of the SWCNT is 10 μm [5, 6]. The angles between two SWCNT bundles are treated as a uniform distribution between [0, 180°]

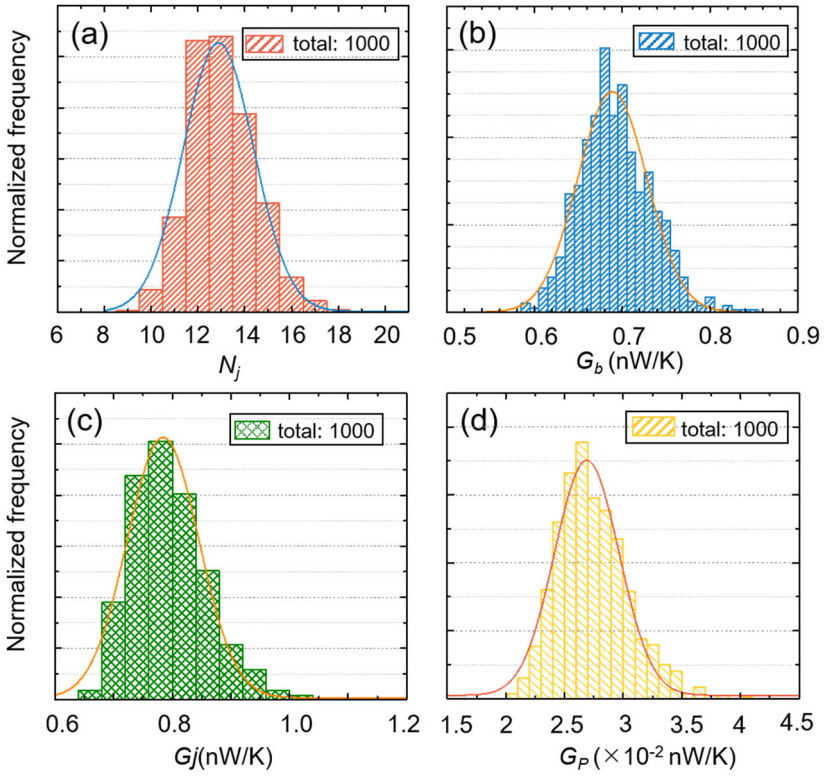

Figure 3. Simulated frequency histogram of (a) Number of junctions in one path. (b) Thermal conductance of bundles consisting one path. (c) Thermal conductance of junctions. (d) Thermal conductance of paths. The average value for the above four parameters are: 13, 0.67 nW/K, 0.78 nW/K and 0.027 nW/K, respectively.

Based on these parameters, 1000 paths from heat source to heat sink are generated randomly for an area of 100 μm × 100 μm. Diameter, length and angle distribution follow the aforementioned distribution. From the 1000 randomly generated paths, frequency histogram for number of junctions per path N_j, thermal conductance per bundle G_b, contact conductance at junction G_j and thermal conductance of path G_P are shown in Fig. 3. Here, the G_b is calculated based on Eq. (2). Besides, thermal conductance of path can also be calculated as:

$$G_p = \left(\left(N_j + 1\right) * \frac{1}{G_b} + N_j * \frac{1}{G_j}\right)^{-1} \qquad \text{Eq. (3)}$$

Using the average value of N, G_b and G_j, the average thermal conductance of path can be estimated with the above equation. The average thermal conductance is nearly the same as the average value in Fig.3 (d). Hence in the following part, Eq. (3) instead of the distribution, will be used to estimate the thermal conductance of the film together with the other three average values.

2.2.1 Bundle length dependence. Figure 4 shows the dependence of G_p on various parameters. In Fig.4 (a), the dependence on bundle length for various G_C is shown. For a fixed G_C, a longer bundle will lead to a higher path thermal conductance while the increasing rate drops when the bundle length reaches to micrometer. For paths consisting of nanometer long bundles, there is a nearly 10 times difference in G_p for different G_C. However, this difference will be reduced with longer bundles and it is reasonable to expect similar G_p when the bundle length keeps increasing. This indicates that the path thermal conductance is dominated by the contact conductance per area when the bundle length is on the order of micrometer.

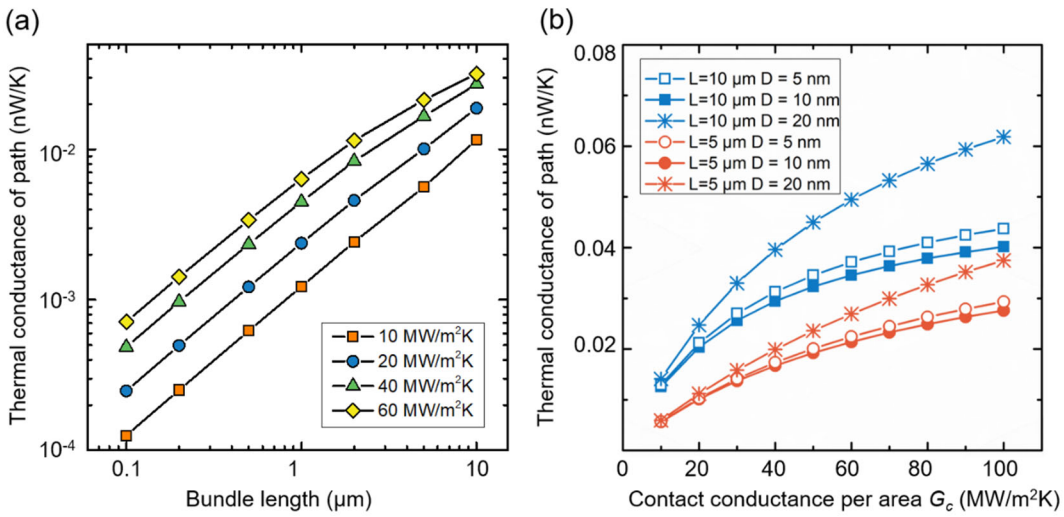

Figure 4. Trend of path thermal conductance with (a) bundle length and (b) contact conductance per area. (a) Four contact conductance per area shows same increasing trend when bundle length varies from 0.1 μm to 10 μm. (b) Bundle length of 5 μm denoted with red lines and 10 μm denoted with blue lines with different contact conductance per area are simulated. For same length, different bundle diameter is distinguished with symbols where hollow symbol, filled symbols and star symbol represent 5, 10 and 20 nm respectively.

2.2.2 Diameter and contact conductance dependence. Figure 4(b) shows the dependence of G_p on the contact conductance per area for various bundle diameters. It is straightforward that the path thermal conductance has a positive dependence on G_C. One thing we want to highlight is that the nonlinear relationship between path thermal conductance and the bundle diameter. In Fig.4(b), when bundle length is fixed, diameter of 10 nm possesses the lowest path conductance compared with the other two diameter, 5 nm and 20 nm. This is because the bundle thermal conductance has a non-linear relationship with bundle diameter, as discussed in Fig.2 (b). For SWCNT bundles, a larger bundle size means more thermal transport channels but also higher possibilities of phonon scattering. The minimum thermal conductance is the result from these two competing factors. For small bundles, scattering phenomenon controls the overall performance, while for large bundles, the number of tubes becomes significant.

2.3. Line density

Another factor in Eq. (1) is N_P, number of effective paths in the film. In the network structure, each SWCNT or bundle is connected with many other SWCNTs or bundles, generating a large number of paths. As discussed above, paths consisting of short SWCNTs or bundles produce low thermal conductivity, contributing little to the film thermal conductance. Therefore, effective thermal transport channels are paths with less junctions. To estimate the number of paths, we introduce line density D_L here. Line density refers to the number of SWCNT or SWCNT bundle crossing one line with a certain length. As the sample size in this study is assumed to be 100 μm × 100 μm, the line density will be discussed on $L = 100$ μm length. For a SWCNT with length of l_i and the angle between horizontal line is θ_i, the possibility of this SWCNT crossing one vertically line will be $2l_i \cos\theta_i / L$. (details are in Supporting information S5(a)) Assuming the number of SWCNT in this region is N_{tube}, and the average bundle size $\bar{n}_b$, the number of bundles N_b can be expressed as $N_{tube}/\bar{n}_b$. The number of bundles that crossing the vertical line could be written as Eq. (4):

$$D_L = \sum_{i=1}^{N_b} \frac{l_i \cos\theta_i}{L} = \frac{\bar{l}}{L} \sum_{i=1}^{N_b} \cos\theta_i = \frac{\bar{l} N_b}{L\pi} \int_{-\frac{\pi}{2}}^{\frac{\pi}{2}} \cos\theta \, d\theta = \frac{2\bar{l} N_b}{L\pi} \qquad \text{Eq. (4)}$$

In our previous experimental research, sheet thermal conductance of four samples with different transparencies have been measured [3]. The transparencies of the four SWCNT film samples are 87%, 72%, 62% and 53%, respectively, at the wavelength of 550 nm. The experiment result will be adopted as benchmark to evaluate the model in this study. The line density of the 87% transparency film (shorted as T87) could be counted from the TEM images. The $D_{L,T87}$ is 38 per 1 μm, that is 3800 per 100 μm. Considering the average length of bundle is 10 μm in Eq. (4), the area density will be around 5.97×10^5. To verify the rationality of this method, we estimated the area density based

on reported papers [8, 34] (Supporting information S5). The calculated SWCNT numbers per 100 μm^2 of the four samples are shown in Fig. S6(b) with pink histogram. Besides, monolayer graphene has been used here to verify the number of carbon atom when having same absorbance with the four SWCNT film. The result is shown in Fig.S6 (b) with green histogram. Although there is small difference among the three methods at each transparency, the order is the same. This gives validity of the line density discussed in here. Therefore, in the following part line density will be used in the model with some modifications to replace number of paths N_P.

Based on the discussion above, equation (1) could be further modified to equation (5), where α is a correction factor.

$$G = \alpha \times D_L \times G_P \qquad \text{Eq. (5)}$$

In the SWCNT film, SWCNTs form plenty of paths and these paths entangle with each other. Two or more effective short paths may have the same starting point, which makes D_L much smaller than N_P, so α is introduced here to compensate this difference. This α is determined by fitting to Eq. (5) with experiment data as shown in Fig.5. Here, when α = 30 it fits well with the experiment data. This indicates that the line density is 30 times smaller than the real number of thermal transport paths. As we have assumed in the previous discussion, many paths of bundles starting from the intermediate positions of a long bundle have less contribution to the thermal conductivity. We can consider that D_L counts all these less important paths compared with the effective paths described by N_p. There are additional two possible reasons for this under-estimation. On one hand, although the SWCNT film is uniform in large scale, as observed in nanoscale regions by TEM, the distribution of SWCNT is not perfectly uniform and this will make the counted line density larger or smaller. On the other hand, from the definition of line density, the possible crossing between these paths are not considered, which is possible for real SWCNT film. These two reasons together lead to an underestimation of the real number of paths. Coincidentally, the deviation between D_L and N_P are similar for all four samples.

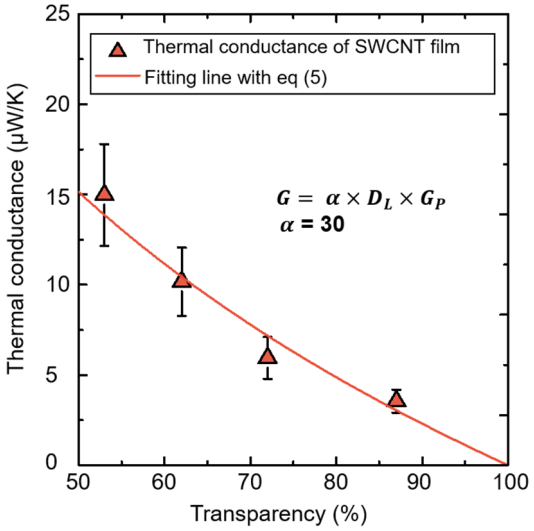

Figure 5. Fitting the model to experiment results. The red triangles are the sheet thermal conductance of four SWCNT samples with different transparency[3]. The red line is fitted with Eq. (5) and α is 30.

3. Thermal transport model of SWCNT-BNNT film

When this model is extended to a SWCNT-BNNT film, α and D_L stay unchanged while G_P will increase because of additional BNNT thermal transport channels. Different from the long extending SWCNTs, the grown BNNTs are separated into small segments by the crossings of SWCNTs in the film, as shown in Fig. 6(a). Length of the BNNT segments follows a lognormal distribution, as shown in supporting information S6. The black lines represent SWCNTs or bundles. The green line is a highlighted SWCNT bundle while the dashed purple lines represent the BNNT walls. For simplicity, BNNT is only shown for highlighted SWCNT. In a SWCNT film, junctions other than those at two ends of a SWCNT have limited influences on the thermal transport along tube axis. In SWCNT-BNNT films, however, these junctions become more important in the model because they divide outer BNNTs into many segments, which will apparently suppress the phonon transport. For the BNNT, segment parts and junction parts connect in series and thermal resistance equation could be written similarly to Eq. (3):

$$G_{BNNT} = ((N'+1) * \frac{1}{G_{BNNT}} + N' * \frac{1}{G_{BN-j}})^{-1} \qquad \text{Eq. (6)}$$

where N', G_{BNNT} and G_{BN-j} are the number of BNNT segments, thermal conductance of BNNT segment and thermal conductance at SWCNT junction, respectively. Thermal conductivity of BNNT is believed to be comparable to or smaller than CNT[35]. However, the thermal conductivity of BNNT is reduced because of the natural isotope abundance of boron. Additionally, the BNNT wrapping SWCNT bundle has a very large diameter. Here we compared thermal conductivities of 500, 1000, 2000 W/mK considering the reported 200 W/mK for large diameter BNNTs[35]. The as-grown BNNT has 2-10 walls, and for simplicity we consider the number of walls to be 4. From the TEM image of SWCNT-BNNT film in Ref. 3, the multilayer BN wrapped the junction tightly and connecting the BNNTs smoothly. Therefore, the G_{BN-j} is ignorable and the BNNT segments are considered to be perfectly connected.

Segment length is needed to calculate the thermal conductance of BNNTs. It is straightforward that the average segment length is proportional to SWCNT density. Thus, segment length is exponentially related to film transparency. The length of segment is tunable and here we assume it to be on the order of hundreds nanometer. It should be noted here that the assumed segment length is larger than what observed in TEM images. This is because TEM images are projections of the film from the top and cannot easily distinguish the depth information, that is, SWCNTs crossing with each other in a TEM image may be separated in thickness direction.

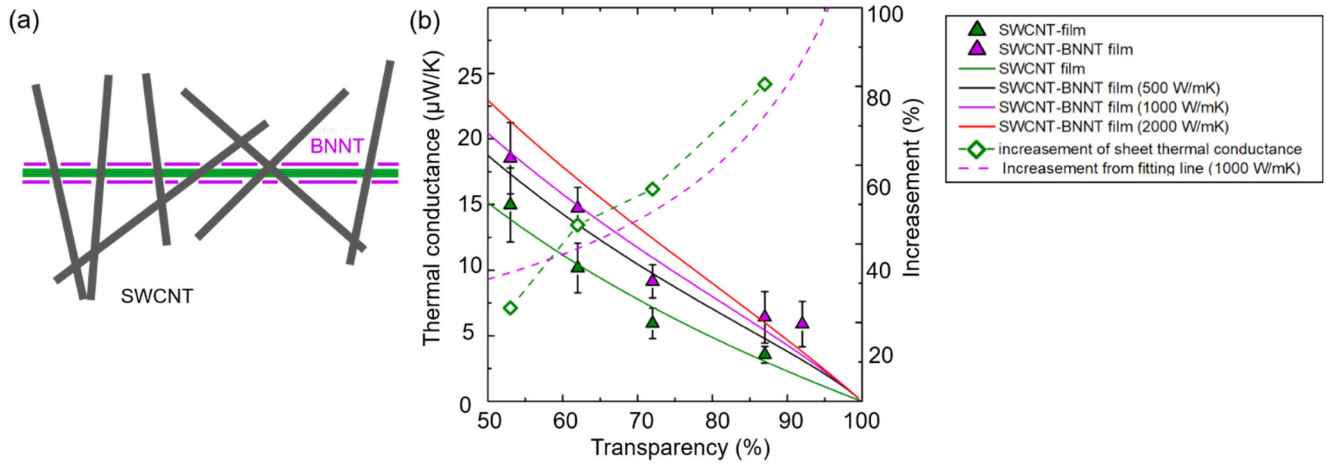

Figure 6. (a) Schematic illustration of the top view the BNNT wrapping SWCNT. The dark grey lines represent SWCNT. Green line is to emphasize one SWCNT coated by short BNNT segmentations denoted by purple lines. (b) Thermal conductance of SWCNT-BNNT heterostructure film[3] and the fitting lines. Black, purple and red lines represent thermal conductance when BNNT thermal conductivity is chosen to be 500, 1000 and 2000 W/mK, respectively. Dashed green line is the increase in thermal conductance before and after BNNT coating from experiment result. Dashed purple line is the predicted increase when BNNT thermal conductivity is 1000 W/mK.

After integrating the above-mentioned condition into Eq. (5), the thermal conductance of SWCNT-BNNT is obtained and plotted in Fig. 6(b) together with the measured thermal conductance. It should be noted here that the line density remains unchanged compared with bare SWCNT film. Compared with the bare SWCNT film, the estimated thermal conductance of SWCNT-BNNT film is improved more efficiently when original SWCNT film has higher transparency, which is in a good agreement with our experiment study [3]. For highly transparent films, the as-grown BNNT segments are longer, rendering smaller N'. The BNNT is treated as connecting with SWCNT bundle in parallel. The smaller the BNNT thermal resistance, hence the smaller the total thermal resistance. However, in thick films, thermal transport channels may consist of bundles in the thickness directions and form long paths from one side to the other, which will lead to more inter-tube junctions. Consequently, a BNNT will be separated into more segments, and large N' will result in a very low BNNT thermal conductance. Another point worth mentioning is that increasing the thermal conductivity of BNNT by two or three times will have limited influence on the estimated film thermal conductance. This means that the contribution of BNNT wrapping to the thermal conductance of the heterostructure film is not originating from offering independent thermal transport channels but making up the weak points in each path. This reveals the most important significance of BNNT coating onto SWCNT networks.

3. Summary

In conclusion, the present work provided a simple model for thermal transport in 2D network of SWCNT bundles. This model could be easily extended to heterostructure films. With some basic statistics such as diameter and length distribution, the film thermal conductance could be estimated. One limitation of this model is that it is not scalable to predict very large size film and all the diffusive discussion will not be valid when the SWCNT is shortened to nanometer. The present model ignore the BNNT influence on SWCNT junctions but we consider this influence is very limited. This model uncovers the principle of thermal transport mechanism in 2D heterostructure films and provides some insights for structure design.

Acknowledgements

Part of this work was supported by JSPS KAKENHI Grant Numbers JP18H05329, JP19H02543, JP20K14660, JP20H00220, JP20KK0114, JST CREST Grant Number JPMJCR20B5, and Shorai Foundation of Science and Technology. We also acknowledge supports from Advanced Characterization Nanotechnology Platform of the University of Tokyo, supported by "Nanotechnology Platform" of the Ministry of Education, Culture, Sports, Science and Technology (MEXT), Japan, grant number JPMXP09A20UT0063.

References

1. Xiang, R., et al., *One-dimensional van der Waals heterostructures.* Science, 2020. **367**(6477): p. 537.
2. Wang, P., R. Xiang, and S. Maruyama, *Chapter Two - Thermal Conductivity of Carbon Nanotubes and Assemblies*, in *Advances in Heat Transfer*, E.M. Sparrow, J.P. Abraham, and J.M. Gorman, Editors. 2018, Elsevier. p. 43-122.
3. Wang, P., et al., *Enhanced In-Plane Thermal Conductance of Thin Films Composed of Coaxially Combined Single-Walled Carbon Nanotubes and Boron Nitride Nanotubes.* ACS Nano, 2020. **14**(4): p. 4298-4305.
4. Yamaguchi, S., et al., *One-directional thermal transport in densely aligned single-wall carbon nanotube films.* Applied Physics Letters, 2019. **115**(22): p. 223104.
5. Nasibulin, A.G., et al., *Multifunctional Free-Standing Single-Walled Carbon Nanotube Films.* ACS Nano, 2011. **5**(4): p. 3214-3221.
6. Hussain, A., et al., *Floating catalyst CVD synthesis of single walled carbon nanotubes from ethylene for high performance transparent electrodes.* Nanoscale, 2018. **10**(20): p. 9752-9759.
7. Jiang, K., Q. Li, and S. Fan, *Spinning continuous carbon nanotube yarns.* Nature, 2002. **419**(6909): p. 801-801.
8. Murakami, Y., et al., *Polarization Dependence of the Optical Absorption of Single-Walled Carbon Nanotubes.* Physical Review Letters, 2005. **94**(8): p. 087402.
9. Penza, M., et al., *Effect of growth catalysts on gas sensitivity in carbon nanotube film based chemiresistive sensors.* Applied Physics Letters, 2007. **90**(10): p. 103101.
10. Qian, Y., et al., *Multifunctional Effect of p-Doping, Antireflection, and Encapsulation by Polymeric Acid for High Efficiency and Stable Carbon Nanotube-Based Silicon Solar Cells.* Advanced Energy Materials, 2020. **10**(1): p. 1902389.
11. Jeon, I., et al., *Single-Walled Carbon Nanotubes in Emerging Solar Cells: Synthesis and Electrode Applications.* Advanced Energy Materials, 2019. **9**(23): p. 1801312.
12. Feng, Y., et al., *Quantitative study of bundle size effect on thermal conductivity of single-walled carbon nanotubes.* Applied Physics Letters, 2018. **112**(19): p. 191904.
13. Kumar, S., M.A. Alam, and J.Y. Murthy, *Effect of percolation on thermal transport in nanotube composites.* Applied Physics Letters, 2007. **90**(10): p. 104105.
14. Nan, C.-W., et al., *Effective thermal conductivity of particulate composites with interfacial thermal resistance.* Journal of Applied Physics, 1997. **81**(10): p. 6692-6699.
15. Volkov, A.N. and L.V. Zhigilei, *Scaling Laws and Mesoscopic Modeling of Thermal Conductivity*

in Carbon Nanotube Materials. Physical Review Letters, 2010. **104**(21): p. 215902.
16. Behnam, A. and A. Ural, *Computational study of geometry-dependent resistivity scaling in single-walled carbon nanotube films.* Physical Review B, 2007. **75**(12): p. 125432.
17. Tsukuda, M., et al., *Random stick network analysis of electronic transport in carbon nanotube thin films.* Applied Physics Express, 2019. **12**(5): p. 055006.
18. Prasher, R.S., et al., *Turning Carbon Nanotubes from Exceptional Heat Conductors into Insulators.* Physical Review Letters, 2009. **102**(10): p. 105901.
19. Chalopin, Y., S. Volz, and N. Mingo, *Upper bound to the thermal conductivity of carbon nanotube pellets.* Journal of Applied Physics, 2009. **105**(8): p. 084301.
20. Volkov, A.N., et al., *Effect of bending buckling of carbon nanotubes on thermal conductivity of carbon nanotube materials.* Journal of Applied Physics, 2012. **111**(5): p. 053501.
21. Jing, L., et al., *Thermal Conductivity Enhancement of Coaxial Carbon@Boron Nitride Nanotube Arrays.* ACS Applied Materials & Interfaces, 2017. **9**(17): p. 14555-14560.
22. He, T., et al., *Mechanical and thermal properties of the coaxial carbon nanotube@boron nitride nanotube composite.* Physica E: Low-dimensional Systems and Nanostructures, 2019. **107**: p. 182-186.
23. Fuhrer, M.S., et al., *Crossed Nanotube Junctions.* Science, 2000. **288**(5465): p. 494.
24. Snow, E.S., et al., *Random networks of carbon nanotubes as an electronic material.* Applied Physics Letters, 2003. **82**(13): p. 2145-2147.
25. Salaway, R.N. and L.V. Zhigilei, *Molecular dynamics simulations of thermal conductivity of carbon nanotubes: Resolving the effects of computational parameters.* International Journal of Heat and Mass Transfer, 2014. **70**: p. 954-964.
26. Pop, E., et al., *Thermal Conductance of an Individual Single-Wall Carbon Nanotube above Room Temperature.* Nano Letters, 2006. **6**(1): p. 96-100.
27. Volkov, A.N., R.N. Salaway, and L.V. Zhigilei, *Atomistic simulations, mesoscopic modeling, and theoretical analysis of thermal conductivity of bundles composed of carbon nanotubes.* Journal of Applied Physics, 2013. **114**(10): p. 104301.
28. Otsuka, K., et al., *Water-assisted self-sustained burning of metallic single-walled carbon nanotubes for scalable transistor fabrication.* Nano Research, 2017. **10**(9): p. 3248-3260.
29. Maruyama S, et al., Anisotropic Heat Transfer of Single-Walled Carbon Nanotubes, J. Therm. Sci. Tech., 2006, 1-2, 138-148.
30. Evans, W.J., M. Shen, and P. Keblinski, *Inter-tube thermal conductance in carbon nanotubes arrays and bundles: Effects of contact area and pressure.* Applied Physics Letters, 2012. **100**(26): p. 261908.
31. Hu, L. and A.J.H. McGaughey, *Thermal conductance of the junction between single-walled carbon nanotubes.* Applied Physics Letters, 2014. **105**(19): p. 193104.
32. Yang, J., et al., *Contact thermal resistance between individual multiwall carbon nanotubes.* Applied Physics Letters, 2010. **96**(2): p. 023109.
33. Zhong, H. and J.R. Lukes, *Interfacial thermal resistance between carbon nanotubes: Molecular dynamics simulations and analytical thermal modeling.* Physical Review B, 2006. **74**(12): p. 125403.
34. Murakami, Y., et al., *Polarization dependent optical absorption properties of single-walled carbon nanotubes and methodology for the evaluation of their morphology.* Carbon, 2005. **43**(13): p. 2664-2676.
35. Chang, C.W., et al., *Isotope Effect on the Thermal Conductivity of Boron Nitride Nanotubes.* Physical Review Letters, 2006. **97**(8): p. 085901.

Supporting Information

Phenomenological model of thermal transport in carbon nanotube and hetero-nanotube films

Pengyingkai Wang[1], Ya Feng[1], Rong Xiang[1], Taiki Inoue[1] Anton Anisimov[2], Esko I. Kauppinen[3], Shohei Chiashi[1], Shigeo Maruyama[1*]

[1] Department of Mechanical Engineering, The University of Tokyo, 7-3-1 Hongo, Bunkyo-ku, Tokyo 113-8656, Japan
[2] Canatu, Ltd., Konalankuja 5, FI‐00390 Helsinki, Finland
[3] Department of Applied Physics, Aalto University School of Science, 15100, FI-00076 Aalto, Finland

E-mail: maruyama@photon.t.u-tokyo.ac.jp

1. Characterization of the three new bundle samples.

SWCNT bundles with different sizes are prepared by the same process as our previous study [1]. Horizontally SWCNTs grown on *r*-cut quartz substrate [2] are transferred to suspended platinum resistance thermometer, followed by annealing at 400 °C for several hours. Only the suspended part of SWCNTs could form bundles while those on the thermometer stay well aligned. The bundle size could be determined by observing the number of SWCNTs extending on the thermometers. In our previous study, sizes of the bundles are: 1, 5, 8 and 13. An apparent decrease in thermal conductivity was observed when bundle size was 5. However, the decreasing trend is difficult to predict without moderate bundle sizes between 1 and 5. In this study, additional three samples with sizes of 2, 3 and 4 were prepared and measured by the same process. Given the same design of micro-thermometer, measurement setup and experiment condition, it is reasonable to put the result of previous study together with this study in the following discussion.

The as-prepared samples are shown in Figure S1. Each bundle is defined by its structure and size. For example, B2 means that the structure is a bundle consisted of two SWCNTs. Figure S1(a), S1(b) and S1(c) are sample B2, B3 and B4, respectively. In SEM images, all suspending bundles are fairly straight and extending long on the two thermometers. Length of the bundle is the gap between two thermometers, which is pre-determined. For all the three samples in this study, the length is 3 μm.

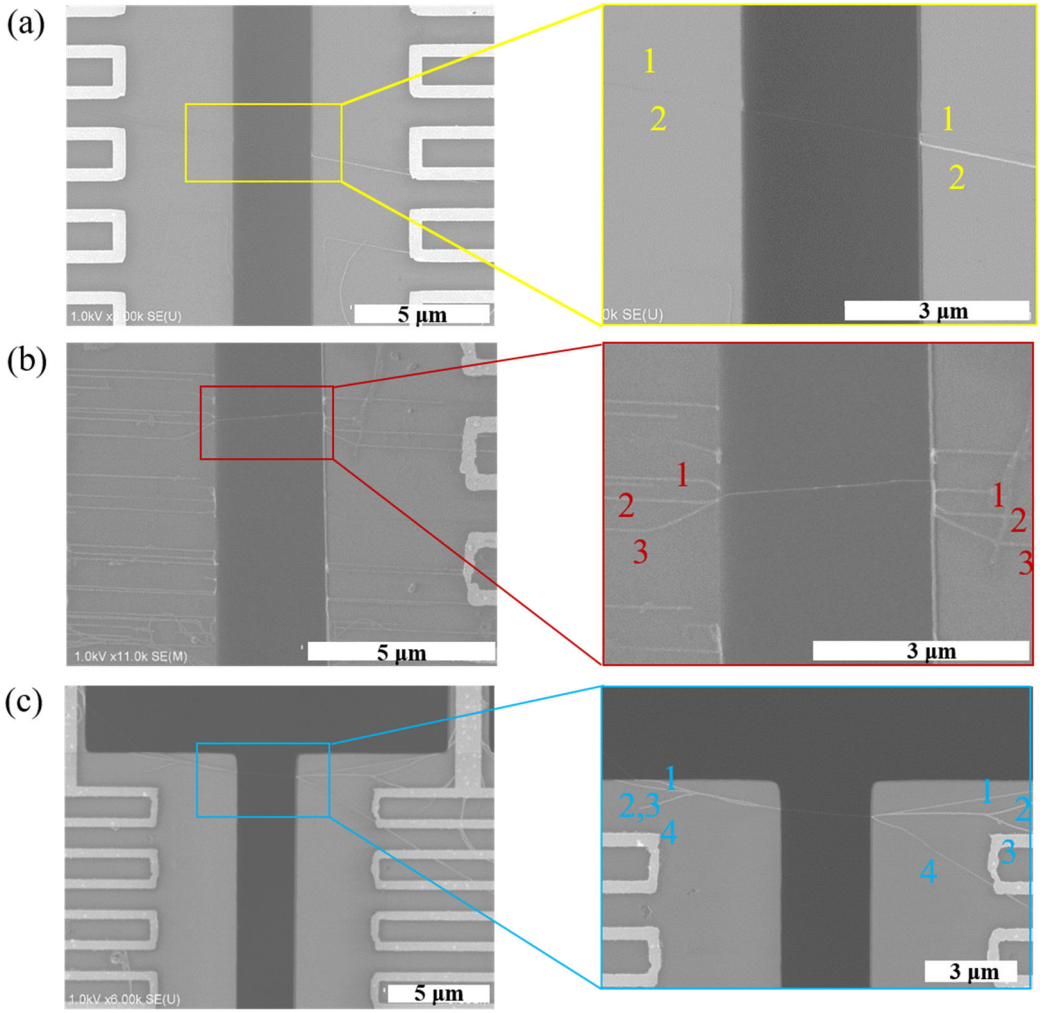

Figure S1. SEM images of three samples. (a) sample B2, gap between two thermometers: 3 μm; (b) sample B3, gap between two thermometers: 3 μm; (c) sample B4, gap between two thermometers: 3 μm.

2. Thermal conductivity of individual SWCNT

The κ_{is} in the fitting lines are plotted against temperature with other two reports in Fig. S2[3]. Here we adopt the equation in Ref.3 and fix the length of the tube to 3 μm in accordance with our experiment. Then the thermal conductivity κ_{is} can be rewritten as $\kappa_{is}\ (T) = (-5.62 \times 10^{-7}T + 23.96 \times 10^{-10}T^2 + 9.3(1 + 0.5/3)T^{-2})^{-1}$, which is a function of temperature. In this way, $\kappa_{bu}(n_b, l, T)$ can be extended to the whole temperature range together with bundle size range.

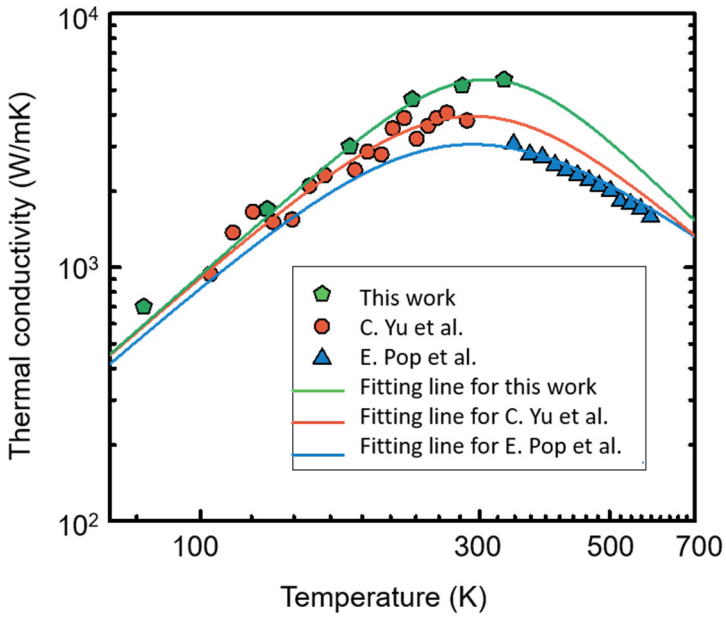

Figure S2. Thermal conductivity of isolated SWCNT as a function of temperature with a fixed length. The colored symbols are thermal conductivity from experiments and the corresponding lines are the estimated thermal conductivity versus temperature with fitting parameters by the model.

3. Frequency histogram of bundle diameter distribution

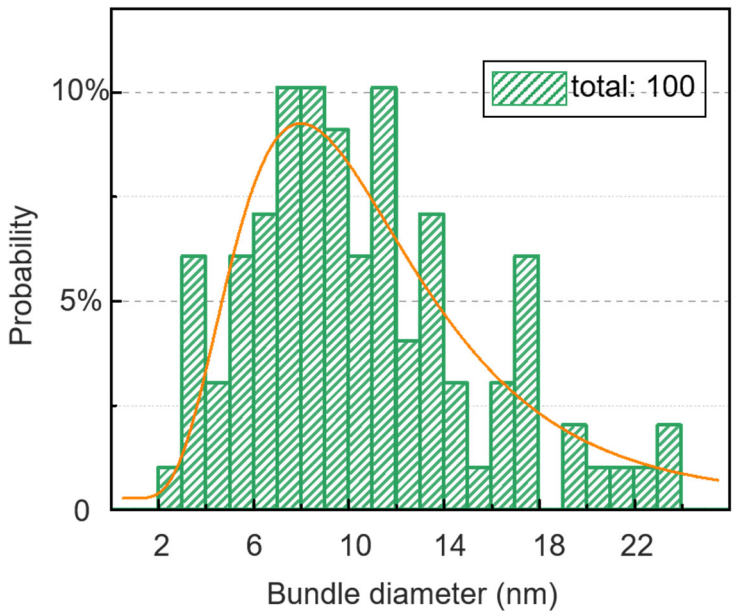

Figure S3. Histogram of the bundle diameter distribution in 87% transparency film. The histogram is fit with the lognormal distribution $d_b \sim Lognormal(2.29, 0.29^2)$

4. Summary of contact thermal conductance per unit area.

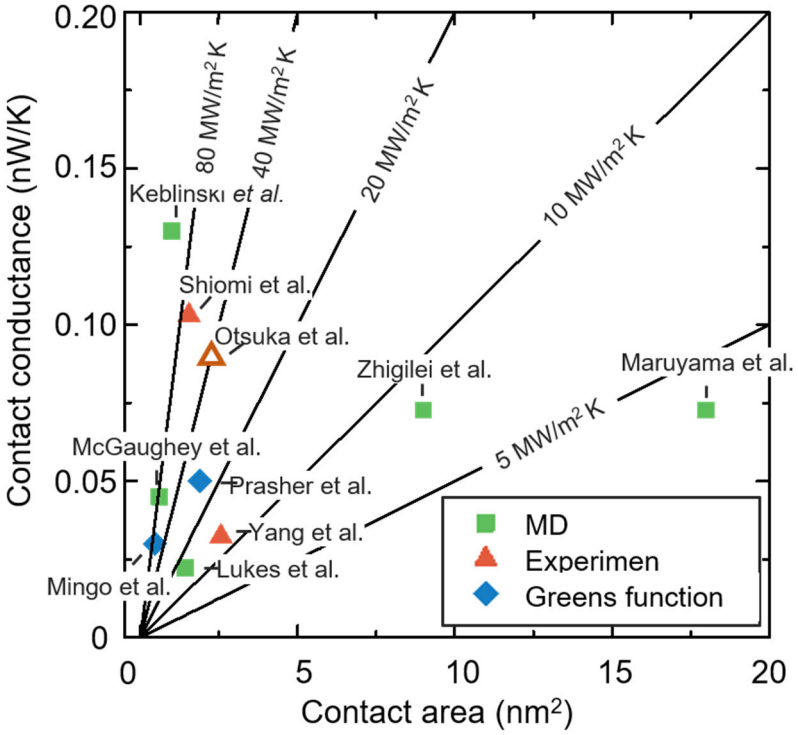

Figure S4. Thermal contact conductance per unit area in previous study[4-13]. The hollow triangle is the SWCNT-substrate contact conductance.

5. Area density estimation with three methods.

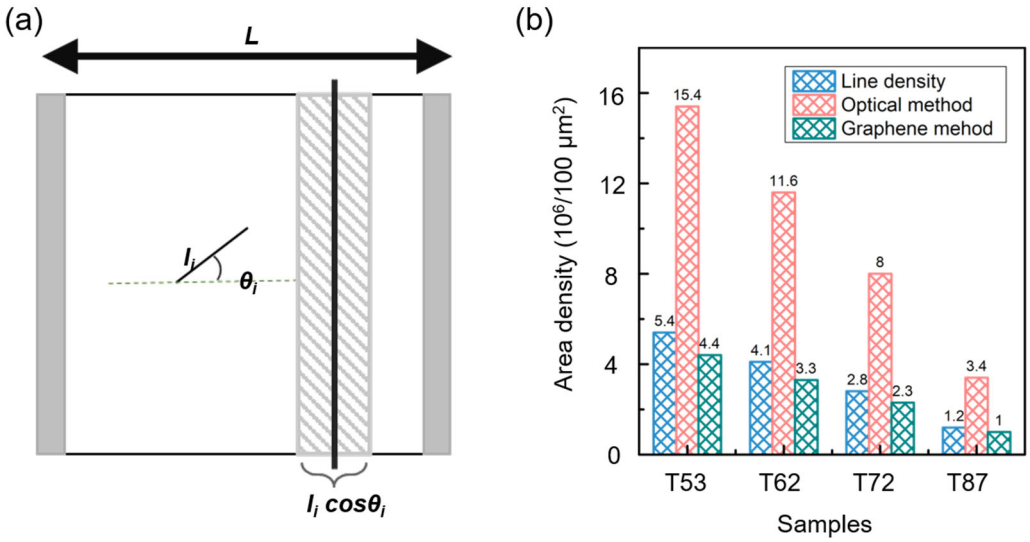

Figure S5. (a) Schematic illustration of SWCNT with the length of l_i falling into the hatched region. Sample is a square of 100 μm×100 μm. θ_i is the angle between the SWCNT and horizontal line, within $[-\frac{\pi}{2}, \frac{\pi}{2}]$. (b) The calculated SWCNT area density from three methods. The blue, pink and green histogram represent area density estimated from line density, optical method and equivalent graphene.

Here we use three ways for estimating the number of CNT in a certain area. (100 μm^2 in this file):

(1) Using line density.

(2) Using Beer–Lambert law based on parameters of SWCNT film.

(3) Using Beer–Lambert law based on parameters of monolayer graphene.

The basic is Beer–Lambert law:

$$\Lambda = -\log_{10} T = \sigma \cdot n \cdot l \tag{1}$$

where Λ is absorbance and T is transmittance. T in this file is chosen as 87%, in consistent with experiment. σ, n, l are bare optical cross-section, molecular concentration of carbon (cm^{-3}) and film thickness, respectively.

The idea is quite straightforward: the number of C atoms in a certain area divided by the number of C atom in a SWCNT is the total number of SWCNTs. For a SWCNT film, σ is adopted from Ref.14, thus $n \cdot l$ for (100 μm)^2 could be calculated, and then the total C atoms in this area is known. For monolayer graphene, area density of C atoms is $3.82 \times 10^{15}/cm^2$.

(1) Based on line density

Line density D_L of 87% transparent film is 3800 μm^{-1}, and each bundle contains n_b = 20 SWCNTs. Combining with Eq. (4) in main text, the total number of SWCNT is:

$$N_{SWCNT1} = \frac{D_L L \pi}{2\bar{l}} \times n_b = 1.19 \times 10^6 \tag{2}$$

(2) Based on optical property of SWCNT film

SWCNT absorption has strong anisotropy. When electric field is applied perpendicularly to the nanotube axis, absorption is drastically reduced by the screen effect of

electric field, called depolarization effect. The absorption of SWCNT is expressed by $cos^2\,\theta$, where θ is an angle between the electric field and a nanotube axis as in the figure.

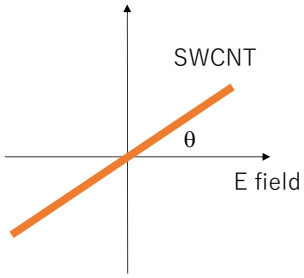

Let's assume that all SWCNT of random network film are straight and in the 2D plane. For random direction of SWCNT, the average absorption for random direction: $\int_0^{2\pi} cos^2\,\theta\,d\theta$, can be compared with fully aligned nanotubes in parallel to the electric field $\int_0^{2\pi} l d\theta = \frac{\pi}{2}$ case. Here, $\int_0^{2\pi} cos^2\,\theta\,d\theta = \frac{1}{2}\int_0^{2\pi}(1+cos\,2\,\theta)d\theta = \frac{1}{2}\left[\theta + \frac{1}{2}sin\,2\,\theta\right]_0^{\theta/2} = \frac{\pi}{4}$. Hence, absorption of random nanotubes relative to parallel polarized case is $\frac{\pi/4}{\pi/2} = \frac{1}{2}$. We can express the cross-section η of random network nanotube as $\eta_{Random} = \frac{1}{2}\sigma_{//}$

The parameters are adopted from Ref.14 where $\sigma_{\|} = 90\ m^2/mol$ at 550 nm (2.25eV) [14]. Then

$$nl = \frac{-\log_{10} T}{\eta_{random}} = 1.32 \times 10^{-11}\ mol/(100\mu m)^2 \quad (3)$$

This will give 4.01×10^{12} carbon atoms in this area. For one SWCNT with diameter d = 2 nm and length l = 10 μm, the number of carbon atom is:

$$n_c = \pi d l N_G = 2.4 \times 10^6$$

Here atom area density N_G is expressed as:

$$N_G = \frac{2(atoms)}{A_{hex}} = \frac{2}{6\frac{\sqrt{3}}{4}{a_{cc}}^2} = \frac{4\sqrt{3}}{9}\frac{1}{{a_{cc}}^2}$$

Therefore, the total number of SWCNT is:

$$N_{SWCNT2} = \frac{nl}{n_c} = 3.37 \times 10^6 \quad (4)$$

(3) Based on optical property of monolayer graphene.

From the previous study on graphene, $\rho_A = 38.2/nm^2$, which is carbon atom area density. For monolayer graphene, transparency is $T_{mono} = 97.7\%$, so carbon atom absorbance is 0.0101. Therefore, for S = 100 μm^2 area, to reach the same transparency of T87 SWCNT film, total number of carbon atom Nc is:

$$N_C = \frac{-\log_{10} T}{-\log_{10} T_{mono}} \times \rho_A S = 2.28 \times 10^{12} \quad (5)$$

Using the number of carbon atoms in one SWCNT $n_c = 2.4 \times 10^6$, the equivalent number of SWCNT is:

$$N_{SWCNT3} = \frac{N_C}{n_c} = 9.53 \times 10^5 \quad (6)$$

Comparing equation (2), (4) and (6), the evaluated number of SWCNTs from line density and monolayer graphene are similar but smaller than optical method result. In general, the absorption cross-section for C atom should depend on the electronic structure of graphene or nanotubes. The absorption spectra are quite smooth at 550 nm (2.25eV) away from band-band transitions, so we could expect the same order of the cross-section for graphene and nanotubes. Graphene can be regarded as ideal no-bundle case. With the increase in bundle size, absorption cross-section should decrease. Hence, the number of SWCNT using the cross-section obtained from larger bundles will be less.

6. BNNT structure and segment length distribution

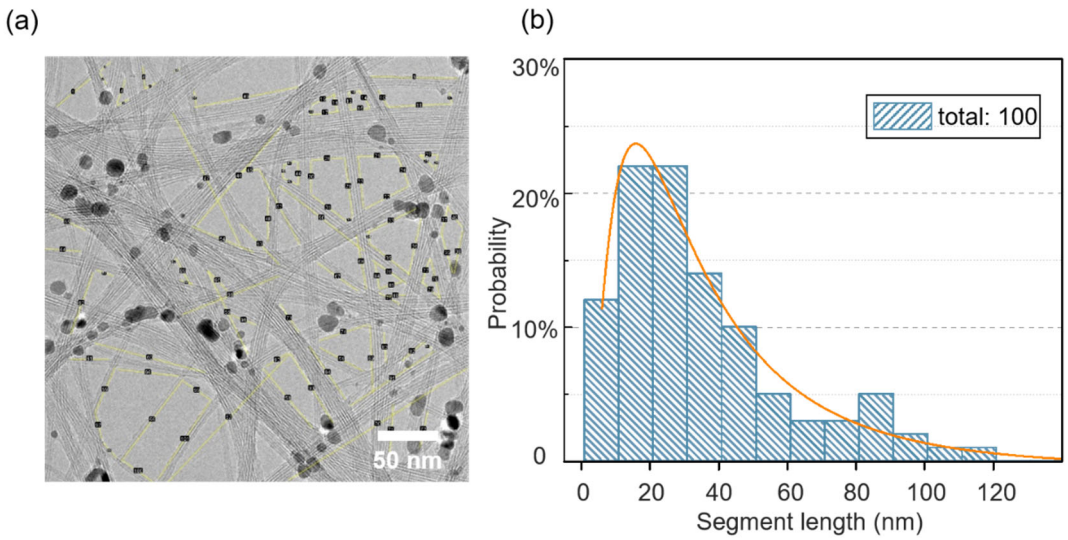

Figure S6. (a) TEM image of the SWCNT-BNNT film. (2) Histogram of the BNNT segment length counted with 100 data point in (a). The length follows a lognormal distribution $Lognormal(3.3, 0.75^2)$.

References:

1. Feng, Y., et al., *Quantitative study of bundle size effect on thermal conductivity of single-walled carbon nanotubes.* Applied Physics Letters, 2018. **112**(19): p. 191904.

2. Chiashi, S., et al., *Growth of Horizontally Aligned Single-Walled Carbon Nanotubes on the Singular R-Plane (10–11) of Quartz.* The Journal of Physical Chemistry C, 2012. **116**(12): p. 6805-6808.
3. Pop, E., et al., *Thermal Conductance of an Individual Single-Wall Carbon Nanotube above Room Temperature.* Nano Letters, 2006. **6**(1): p. 96-100.
4. Volkov, A.N., R.N. Salaway, and L.V. Zhigilei, *Atomistic simulations, mesoscopic modeling, and theoretical analysis of thermal conductivity of bundles composed of carbon nanotubes.* Journal of Applied Physics, 2013. **114**(10): p. 104301.
5. Otsuka, K., et al., *Water-assisted self-sustained burning of metallic single-walled carbon nanotubes for scalable transistor fabrication.* Nano Research, 2017. **10**(9): p. 3248-3260.
6. Maruyama, S., et al., Anisotropic Heat Transfer of Single-Walled Carbon Nanotubes, J. Therm. Sci. Tech., 2006, **1(**2), p. 138.
7. Evans, W.J., M. Shen, and P. Keblinski, *Inter-tube thermal conductance in carbon nanotubes arrays and bundles: Effects of contact area and pressure.* Applied Physics Letters, 2012. **100**(26): p. 261908.
8. Hu, L. and A.J.H. McGaughey, *Thermal conductance of the junction between single-walled carbon nanotubes.* Applied Physics Letters, 2014. **105**(19): p. 193104.
9. Yang, J., et al., *Contact thermal resistance between individual multiwall carbon nanotubes.* Applied Physics Letters, 2010. **96**(2): p. 023109.
10. Chalopin, Y., S. Volz, and N. Mingo, *Upper bound to the thermal conductivity of carbon nanotube pellets.* Journal of Applied Physics, 2009. **105**(8): p. 084301.
11. Zhong, H. and J.R. Lukes, *Interfacial thermal resistance between carbon nanotubes: Molecular dynamics simulations and analytical thermal modeling.* Physical Review B, 2006. **74**(12): p. 125403.
12. Yamaguchi, S., et al., *One-directional thermal transport in densely aligned single-wall carbon nanotube films.* Applied Physics Letters, 2019. **115**(22): p. 223104.
13. Prasher, R.S., et al., *Turning Carbon Nanotubes from Exceptional Heat Conductors into Insulators.* Physical Review Letters, 2009. **102**(10): p. 105901.
14. Murakami, Y., et al., *Polarization Dependence of the Optical Absorption of Single-Walled Carbon Nanotubes.* Physical Review Letters, 2005. **94**(8): p. 087402.